Improving Compression Recovery of Foam-formed Fiber Materials

Sara Paunonen,* Oleg Timofeev, Katariina Torvinen, Tuomas Turpeinen, and Jukka A. Ketoja

Foam technology enables the preparation of new fiber-based materials with reduced density and improved mechanical performances. By utilizing multi-scale structural features of the formed fiber network, it is possible to enhance the elasticity of lightweight cellulose materials under compressive loads. Sufficient strength is achieved by optimally combining fibers and fines of different length-scales. Elasticity is improved by adding polymers that accumulate at fiber joints, which help the network structure to recover after compression. This concept was demonstrated using natural rubber as the polymer additive. For a model network of viscose fibers and wood fines, the immediate elastic recovery after 70% compression varied from 60% to 80% from the initial thickness. This was followed by creep recovery, which reached 86% to 88% recovery within a few seconds in cross-linked samples. After 18 h, the creep recovery in those samples was almost complete at up to 97%. A similar improvement was seen for low-density materials formed with chemi-thermomechanical fibers. The formed structure and elastic properties were sensitive not only to the raw materials, but also to the elastomer stiffness and foam properties. The improved strain recovery makes the developed cellulose materials suitable for various applications, such as padding for furniture, panels, mattresses, and insulation materials.

Keywords: Fibrous materials; Cellulose; Elasticity; Compression; Recovery; Foam forming

Contact information: VTT Technical Research Centre of Finland Ltd, Solutions for Natural Resources and Environment, Tekniikankatu 1, Tampere, P.O. Box 1300, FI-33101 Tampere, Finland;
** Corresponding author: sara.paunonen@vtt.fi*

INTRODUCTION

Foam forming is a technique that uses wet foam instead of water to deposit fibers and bond them into networks. In simple terms, it combines the ability of water to act as a strong cellulose binder with the ability of bubbles to tailor a porous structure and prevent fiber flocking. Lately, the technology has been intensely studied in the preparation of sheet structures (Radvan and Gatward 1972; Lehmonen *et al.* 2013) and bulk materials (Madani *et al.* 2014; Alimadadi and Uesaka 2016) made from wood fibers, especially for filtering (Heydarifard *et al.* 2016) and insulating applications (Poranen *et al.* 2013; Pöhler *et al.* 2016). Forming and subsequent water removal and drying methods have a profound effect on the sheet structure (Timofeev *et al.* 2016; Haffner *et al.* 2017). Foam-formed fiber networks can have a much lower density (Madani *et al.* 2014), improved and tailored pore size distribution (Al-Qararah *et al.* 2015a), and more diverse fiber orientation (Alimadadi and Uesaka 2016) compared with similar water-formed materials.

Foam-formed three-dimensional wood fiber networks (3DFNs) have structural similarities with sheet materials, such as paper. The load-bearing elements in both are the

same: fibers, joints, and a connected network. Paper exhibits three types of deformation: linear and non-linear elastic strain, visco-elastic time-dependent recoverable creep, and plastic non-recoverable deformation (Brezinski 1956; Alava and Niskanen 2006). Alimadadi and Uesaka (2016) reported the same phases for foam-formed 3DFNs made from pure thermomechanical (TMP) reject pulp.

However, the fiber network structure of 3DFNs is very different from that of sheets. The number of bonds a fiber makes with neighboring fibers at low densities is different from that for thin sheets. 3DFNs also retain their integrity more easily than sheets (Alimadadi and Uesaka 2016). Moreover, 3DFNs show a unique and much higher deformation recovery compared with paper and some nonwoven sheets. This is because of the wider 3D fiber orientation distribution and the large proportion of very large open pores in the fiber network. Individual fibers can bend without local geometric restrictions; thus, they avoid stress buildup that drive plastic deformation. In denser networks of natural fibers, only a small proportion of the fibers contributes to the load bearing (Kulachenko and Uesaka 2012), which leads to a highly concentrated stress buildup and plastic deformation. In addition to the number of bonds (determined by the material density) (Borodulina *et al.* 2012; Borodulina *et al.* 2016), the stress and strain distribution in a material is affected by several other factors, such as the fiber length and stiffness, and bond compliance and strength.

The goal of this study was to find methods to improve the elastic and viscoelastic creep recovery of foam-formed 3DFNs and extend their use to application areas where highly flexible and elastic materials are preferred. Examples of such applications are padding for furniture, panels, shoes, pillows, mattresses, and insulation materials. Ideally, these materials would exhibit a sponge-like spring-back behavior after repeated compression cycles. The hypothesis of the authors was that this can be achieved by optimally combining: 1) a low-density structure containing large, open pores obtained by foam forming, 2) a multi-scale fiber network with structural elements of different length-scales (fibers and fines), and 3) an elastic polymer component that accumulates at the fiber joints during drying and helps the network structure to recover after deformation. Figure 1 summarizes the postulated behavior of a 3DFN from foamed furnish to dry material. When water is removed during drying, the suspended polymer component accumulates at the fiber joints, which causes an increase in the network recovery after deformation.

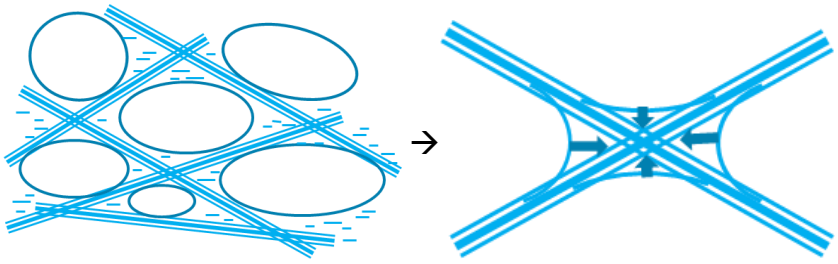

Fig. 1. Schematic illustration of the hypothesis. Left: Wet foam with air bubbles (circles), fibers (bars), and an added polymer component (short lines) during foam forming; Right: Accumulation of the polymer at fiber joints during drying

The foam properties have a considerable effect on the properties of a material. The material density can be reduced by increasing the air content of the wet foam (Madani *et al.* 2014), which also improves the foam stability. Additionally, the mean pore size can be controlled by the bubble size and fiber stiffness (Al-Qararah *et al.* 2015a). Fine particles

and polymers are carried in bubble vertices and interfaces. The surface tension drives the free water towards fiber crossings during drying, which also causes the accumulation of the elastic polymer at these regions. In the fully dried material, the polymer helps the network recover after deformation.

In this study, the hypothetical behavior was studied *via* two model systems in which the above ingredients were present. In the first system, non-bonding flexible viscose fibers were combined with a new type of lignin-containing wood fines material (Saharinen *et al.* 2016). This allowed separate control of the long-fiber density and bonding ability. The second system was based on a more typical stiff fiber material, called chemi-thermomechanical pulp (CTMP).

Natural rubber was used as a model polymer, as it is known to bind to the surface of cellulose (Flink *et al.* 1988). Binding can be further improved through chemical surface modification (Kato *et al.* 2015). Natural rubber has been previously used as a matrix polymer in cellulose fiber-reinforced composites (Kato *et al.* 2015; Zhou *et al.* 2015). The approach of this study was similar to that of earlier studies, but the target material densities were much lower. The density of vulcanized rubber (920 kg/m^3 to 1200 kg/m^3) (McPherson 1927) is lower than that of cellulose crystals (1500 kg/m^3) (Alava and Niskanen 2006), which makes natural rubber an appealing polymer for lightweight fiber materials. Moreover, aqueous foam provides a natural carrier for hydrophobic and non-polar rubber polymers to adhere to the air bubbles in the foam during structure forming. Strong binding of the polymers with lignocellulosic fibers and fines was achieved in the final structure without any chemical modification.

The objective of this study was to assess the effects of the furnish composition, polymer content and crosslinking, and foam properties on the compression recovery of foam-formed 3DFNs.

EXPERIMENTAL

Materials

Two types of long-fiber material were used to prepare the samples (Fig. 2). The staple viscose fiber material (Danufil, Kelheim Fibres GmbH, Kelheim, Germany) had a fiber length of 6 mm and a linear mass density of 1.7 dtex (mass in g/10000 m). The fiber cross-section was roughly elliptical with a major axis diameter of 17.5 µm. The material had a moisture content of 50%. The spruce CTMP, which had an average (length-weighted) fiber length of 1.6 mm and a freeness of 570 mL, was obtained from a Finnish paper mill. The CTMP included a large amount (approx. 30 w/w%) of sub-micron fine particles, *i.e.* fines.

A new type of lignocellulosic fines material prepared by grinding wood (Saharinen *et al.* 2016), called v-fines (Fig. 2), was used at a consistency of 2.5% with the viscose fibers. The special V-patterned surface of the grinding stone enables a 90% conversion of the wood directly into fines in one process step. Consequently, in addition to cellulose, the fines also contain hemicellulose and lignin. The average (length-weighted) length of the v-fines was 0.18 mm, and 71% of the particles were less than 0.2 mm in length.

The aqueous natural rubber latex (Liquid Latex Direct, Burton-upon-Stather, UK) had a total solids content of 60.3% (of which 0.38% was ammonia) and a pH of 10.6. Natural rubber is a polymeric hydrocarbon produced by some tropical plants (Kohjiya and Ikeda 2014) and is collected from trees as an aqueous latex. Vulcanization cross-links

polymers and leads to an elastic and less-sticky rubber (Kohjiya and Ikeda 2014; Kato *et al.* 2015). In this study, the pre-vulcanized latex contained a dye to aid in the analysis of the macroscopic latex distribution in the samples after their production. The preliminary vulcanization was further enhanced by adding sulfur (Sigma-Aldrich, St. Louis, MO, USA), which was either in colloidal or powder form, and employing a 10-min heat treatment at 155 °C.

The samples were prepared using two different types of foaming agent: 10 w/w% solution of anionic sodium dodecyl sulfate (SDS; $C_{12}H_{25}SO_4Na$) (Sigma-Aldrich) with a purity of 90% and a non-ionic surfactant (TWEEN 20, Sigma-Aldrich).

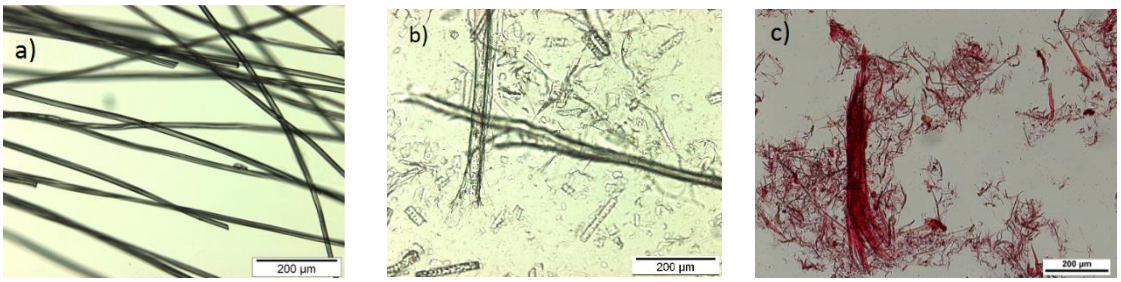

Fig. 2. Raw materials: a) viscose fibers, b) CTMP fibers and fines, and c) v-fines

Methods

Sample preparation

A sequence of model samples was prepared with the non-bonding viscose fibers and v-fines as the main raw materials. The goal was to vary the sample density, fiber binding properties (with v-fines), latex content and stiffness (by vulcanization), and surfactant type. The furnish compositions are summarized in Table 1. The second series with CTMP (Table 2) was used to demonstrate the compression behavior of normal pulp.

Table 1. Composition of the Samples with Viscose Fibers and V-fines

ID	Viscose [g]	V-fines [mL]	Latex: 60% [mL]	Sulfur [g]	Tween [mL]	SDS: 10% [mL]	Water [L]	Density* [kg/m^3]
V1[i]	33	74	20	--	--	1.2	0.17	64.4
V2	46	23	14	--	--	1.2	0.17	46.9
F1	23	23	14	--	--	1.2	0.17	27.0
F2	23	12	14	--	--	1.2	0.17	22.9
L1[ii]	23	23	--	--	--	1.2	0.17	73.0
L2	23	23	7	--	--	1.2	0.17	97.7
L3	23	23	10	--	--	1.2	0.17	38.2
S1	23	12	14	5.0[iii]	--	1.2	0.17	34.3
S2	23	12	14	5.0[iv]	--	1.2	0.17	35.8
S3	23	12	14	5.0[iv]	18	1.0	0.17	31.7

[i] Only underwent repeated compression test (after 18 h); [ii] Only underwent first compression test; [iii] Colloidal sulfur, [iv] Powder sulfur; * At standard climate (23 °C and 50% relative humidity (RH))

Table 2. Composition of the Samples with CTMP

ID	CTMP [g]	Latex: 60% [mL]	Sulfur [g]	Tween [mL]	SDS: 10% [mL]	Water [L]	Density* [kg/m^3]
C1	11.5	--	--	--	1.8	0.25	20
C2	7.5	--	--	--	1.5	0.25	13
C3	7.5	6.3	--	10.0	--	0.25	14
C4	7.5	--	--	6.3	--	0.25	13
C5	7.5	25	--	12.5	--	0.25	19
C6	7.5	12.5	7.5	12.5	--	0.25	29
C7	5.0	18.8	5.0	12.5	--	0.25	27

* At non-standard conditions (approx. 30% RH)

The preparation of the viscose samples (Table 1) began by foaming water together with the surfactant up to an approximate volume of 1000 mL with a mixer (ShearMaster, Netzsch, Hedensted, Denmark) at a rotational speed of 3500 rpm. The corresponding air content was thus very high, around 83%, which improved the foam stability. If the composition contained v-fines, the latex and fines were mixed prior to combination with the long fiber fraction. The whole furnish was subsequently mixed gently by hand. The obtained furnish was then poured into the ready-made foam (to avoid flocculation of the long fibers) and mixed at the same rotational speed used initially (duration = approx. 3 min). The foam volume remained quite stable during the latter mixing. The obtained fiber foam was then poured into a metal cylinder laying on a metallic forming fabric. To ease removal of the sample, the inner surface of the cylinder was covered with release paper. Water was removed first by drainage through the bottom fabric for about 10 min, and then by drying overnight at 100 °C in an oven. During drying, the vapor flow could easily cause the accumulation of latex on the outer surface of the sample. This problem became worse if the latex content and sample density were higher, which caused sample pores of the latex films to close. In the studied low-density samples, this was largely avoided by the very open pore structure and binding the latex with the fines material. If the composition contained sulfur, the rubber was vulcanized by holding the sample at a temperature of 155 °C for 10 min.

The CTMP samples (Table 2) were prepared in the same way, but instead of adding the furnish into a ready-made foam, the shorter CTMP fibers, surfactant, and latex were all foamed using one mixing operation only.

The dry samples had a diameter of 98 mm and a height that ranged from 20 mm to 90 mm. The viscose samples were tested the following day at the earliest after preparation and a minimum of 2 h of conditioning at a standard climate (23 °C and 50% RH). The CTMP samples were tested at non-standard conditions with a similar temperature and lower RH (approx. 30%).

Mechanical testing

Cyclic compression tests of the main sample series (Table 1) were run on a Lloyd tester (Model LR 10K, Lloyd Instruments/Ametek, West Sussex, UK) with compression stages of 10%, 30%, 50%, and 70% of the sample height. The samples were tested without precutting after drying. The test speed was 10%/min for the first cycle, and 100%/min for the subsequent cycles.

There was a non-loaded hold time of 60 s between the cycles. From each cycle, the immediate elastic strain recovery from the top load down to a load of 106 Pa was recorded. By further reducing the load to a nearly 0-Pa pressure, the creep recovery over a period of a few seconds could be measured. The samples were tested again after a rest period of 18 h. The long-term creep recovery was simultaneously measured. For the CTMP samples, the compression levels were slightly different from the main series, and were 20%, 50%, 70%, and 90%. Instead of measuring the spring-back over a few seconds only, the creep recovery was followed over an extended period of 1800 s after compression.

Independent tensile tests of the mechanical properties of the dried rubber were also performed on the Lloyd tensile tester. Rubber bands (50 mm x 15 mm) were tested at a straining rate of 120 mm/min (without sulfur) or 180 mm/min (vulcanized). From these tests the elastic moduli of the dried rubber before and after vulcanization were obtained.

Sample thickness and weight

The thickness was recorded during the compression test at the 106-Pa load level. Upon reaching 106 Pa, the large-scale unevenness and small-scale roughness were evened out. Under this load, the test plate and touched most of the top of the sample, but did not yet compress its body. The weight was recorded immediately after drying (fully dried sample) and at a standard climate before compression testing for the density calculation.

High-speed dynamic imaging

The deformation mechanisms during compression were visualized using high-speed charge-coupled device imaging (Y3, IDT, Tallahassee, FL, USA) of the side of the sample. The imaging frequency was 1000 Hz with a 12-µm pixel size and a pixel resolution of 1280 x 1024. Because of the high imaging frequency, very strong light sources were necessary to ensure sufficient lighting to record the images. Because of the very low sample density and the open porous structure, the fiber network deformations were quite visible with this method.

Micro-computed X-ray tomography

Micro-computed X-ray tomography (XµCT) (Stock 2008) is a method for obtaining a digitalized 3D representation of basically any material, even fragile samples (Salvo *et al.* 2003). The method produces a 3D density map that also records the interior of the sample without disintegrating it. The typical sample size ranges from millimeters to a few centimeters for common XµCT devices.

Micro-computed X-ray tomography imaging is based on X-ray attenuation maps (shadowgrams) obtained from multiple positions around the sample. By using an inverse Radon transform, a digital representation of the original 3D structure of the sample can be reconstructed from a shadowgram series (Kak and Slaney 2001). As X-rays are sensitive to the material density, the resulting 3D image matrix shows the density differences in the sample.

To investigate the internal structure and porosity of the samples, XµCT images (1172, Skyscan/Bruker, Kontich, Belgium) were produced for the S2, S3, and C6 samples. As latex is less dense than cellulose fibers, XµCT can be used for detecting the amount and spatial distribution of latex. The sample size was 2 mm x 2 mm x 2 mm.

RESULTS AND DISCUSSION

Structural Properties

Regenerated viscose fibers from cellulose have considerably different structures and properties compared with natural wood fibers. The viscose fibers are manufactured as a single straight filament and cut to length, which generally leads to a smooth surface and uniform cross-section. In contrast, mechanical CTMP contains fibers with a wide length distribution, as well as fines. The rough surface of wood fibers is fibrillated because of the mechanical forces of the pulping process. Additionally, CTMP fibers have a different cellulose crystal structure and stiffness compared with regenerated cellulose fibers (Nishino *et al.* 1995). Both fiber types are hydrophilic, but their bonding properties differ greatly. While CTMP fibers and wood fines bond strongly *via* hydrogen bonding and other short-range forces, viscose fibers show practically no bonding because of the very small contact area between their rounded surfaces. Therefore, viscose fibers provide a model fiber network that allows the bonding strength to be increased systematically by the addition of fines material and latex to the network.

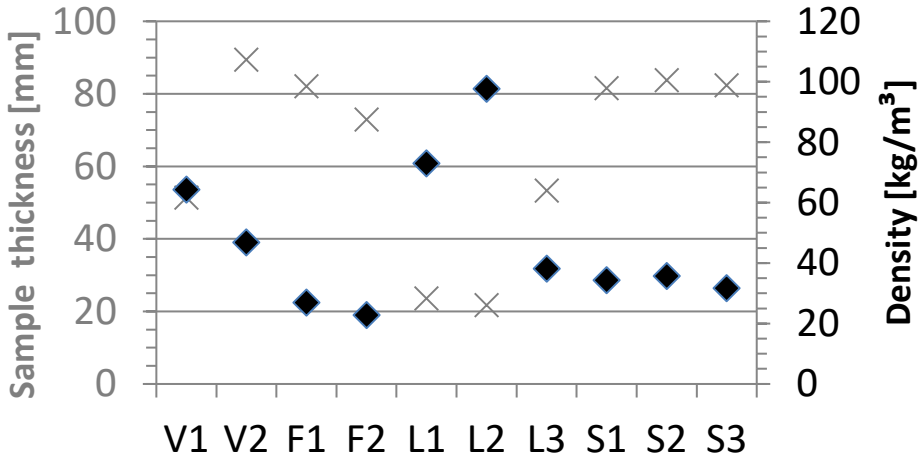

Fig. 3. Thickness and equilibrium density of the viscose samples

The sample thickness varied from 20 mm to 90 mm, as can be seen in Fig. 3. The low thickness of samples L1 and L2 was because of their collapse during the drainage phase, which was probably caused by their low (L2) and zero (L1) latex contents. Before drainage, the air contents of the L1 fiber foam (87%) and L2 fiber foam (85%) were higher than the air contents of the other samples. Moreover, the retention of v-fines was estimated to be very high, around 95%, in a sample without latex. Thus, the latex already seemed to contribute to the strength of the viscose fiber network in the wet state. The collapsed samples were not analyzed further. The foam for sample L3 had a lower air content (66%) than the remaining samples (approx. 83%) and some relatively big bubbles, which manifested as a low sample thickness. The V1 sample with its high v-fines content also had a lower thickness compared with the average, but the results were kept in the series. The densities of the remaining samples (V2 to F2, and S1 to S3) were comparable to those of fibrous building insulation materials.

The XμCT images of samples S2 and S3 in Fig. 4 give an insight into the appearance of the network and how the latex was distributed within it. Viscose fibers

appeared in bundles in the network. There were two possible causes for this. The wet fiber bundles may not have fully dispersed during fiber foam mixing, as the bundles might have been reinforced by the latex. Moreover, because of the smooth fiber surfaces, they interacted less with the foam bubbles compared with natural fibers (Al-Qararah *et al.* 2015b). Similar bundles were not observed in the samples with CTMP fibers. Another possibility was that during sample preparation, the foam bubbles pushed the fibers together. Such a phenomenon is possible in principle, as the close inter-bubble contacts in foam, which have very high air contents, create narrow intermediate spaces for the fibers. Whatever the reason, the viscose fibers remained in bundles during drainage and drying, which resulted in large empty voids. This is shown in Fig. 4a. The general orientation of the fibers was vertical, although some fibers (and fiber segments) diverged greatly from this orientation. This alignment of fibers was probably caused by the vertical flow direction when filling the mould with the wet foam.

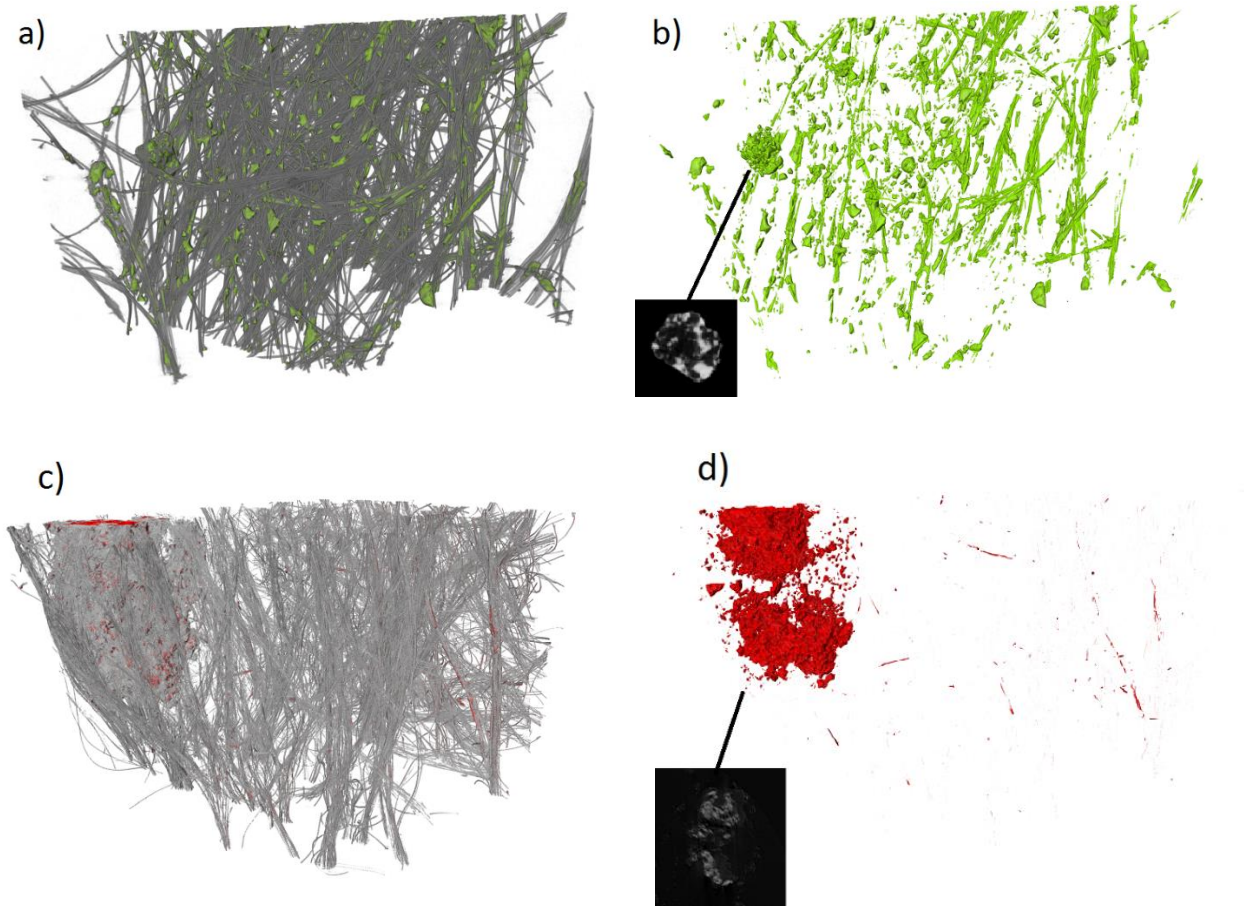

Fig. 4. XµCT images of samples S3 (a and b) and S2 (c and d): a) S3 network structure with viscose fibers (grey) and natural rubber latex (green); b) Latex distribution within the same region of a) with a blow-up that shows the fine structure of a particle formed by the latex (light grey) and v-fines (dark grey); c) S2 network structure with viscose fibers (grey) and natural rubber latex (red); and d) Latex distribution inside the same region of c) with a blow-up of the fine-structure of a big particle with v-fines and latex. Image size: 2 mm x 2 mm x 2 mm.

Figure 4b shows the distribution of latex within the structure of sample S3. Instead of covering the fiber surfaces uniformly, the latex accumulated, especially at fiber crossings and within the fiber bundles. In particular, much of the surface corresponding to

free fiber segments was not covered by latex at all. In other words, the distribution of the latex was qualitatively quite similar to the ideal picture presented in Fig. 1. Thus, a remarkable effect on the mechanical properties and recovery from compression could be expected.

Figure 4b also includes a blow-up picture of a large particle visible in the structure. The cross-sectional image shows that the particle was not homogeneous. To facilitate a high retention of latex, it was pre-mixed with v-fines before being added to the furnish. These components formed a tightly-bound compound particle that survived the shear forces generated during foam preparation. These types of agglomerates did not take part in the load bearing of the network, but still indicated a strong affinity between the latex and wood fiber materials.

The extent of agglomeration depended on the type of surfactant. The formed compound particles were quite small for the mixture of the neutral TWEEN surfactant and the anionic SDS. In this case, the hydrophobic interaction probably drove a proportion of the latex polymers to the bubble interfaces and replaced neutral surfactant molecules there, which left a smaller proportion of latex to form possible compounds with the v-fines. In contrast, sample S2, made purely with the anionic SDS surfactant, contained almost macroscopic compound particles, which contained a very large proportion of the latex. This can be seen in Figs. 4c and 4d. It was possible that the SDS polymers with a hydrophobic tail bonded to the interfaces more strongly than the neutral surfactant, which left the latex polymers free to migrate inside the foam and agglomerate with the v-fines.

The XµCT images enabled calculation of the porosity and volume fractions of the cellulose and latex components. The total porosity of the S3 region shown in Fig. 4a was 0.973. Of the remaining solids, the volume fraction of latex was 22%. Using the known densities of cellulose II (1520 kg/m^3) and natural rubber with a high sulfur content (1200 kg/m^3) (McPherson 1927) led to a mass fraction estimate of 19 w/w% for the latex. The effective density of all of the solids and water was equal to 1400 kg/m^3, which was calculated based on an 8.2% moisture content in the fibers at 50% RH. By comparing this effective density with the measured average density of the sample, a porosity value of 0.977 was obtained, which was quite close to the direct estimate stated above. The retention of the latex based on the above estimates was 41% for sample S3.

For sample S2, the porosity estimate based on Fig. 4c was 0.955 with an 8.2% latex volume fraction. Similar calculations to the above led to a mass fraction estimate of 6.8 w/w% for sample S2. However, the structural heterogeneity of the sample was large, and therefore there was some uncertainty in the above estimates. In particular, a part of the latex seemed to migrate to the outer surfaces of the sample, where it was visible as a higher color intensity. This migration probably caused the low latex content inside of the sample.

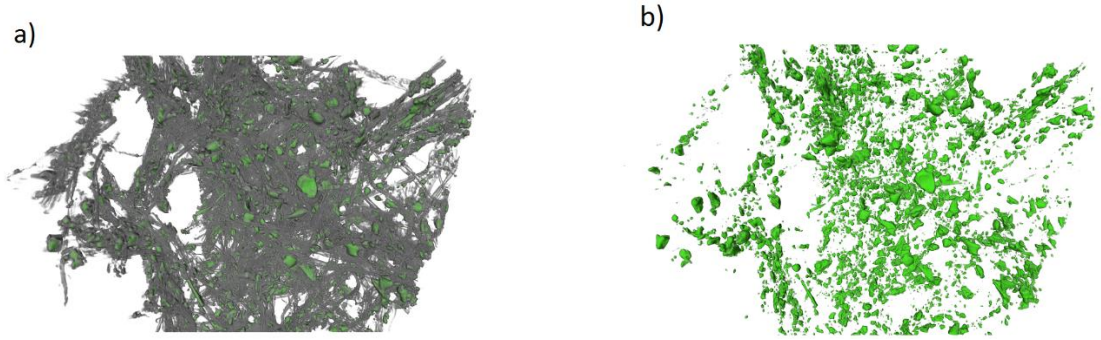

Fig. 5. XµCT images of CTMP sample C6 (a) and the corresponding latex distribution (b)

Preparation of the CTMP samples was more difficult, as the latex was not pre-mixed with the fines and could therefore migrate to the surfaces during drying. With a low enough fiber density, successful samples were still obtained with a similar distribution of latex inside the fiber network (Fig. 5), as was the case for the viscose samples. The estimated latex volume fraction in sample C6 was 28.5%, which corresponded to a 25 w/w% mass fraction.

Compression Recovery

Figures 6 andFig. 7 summarize the elastic behavior observed in the cyclic compression tests.

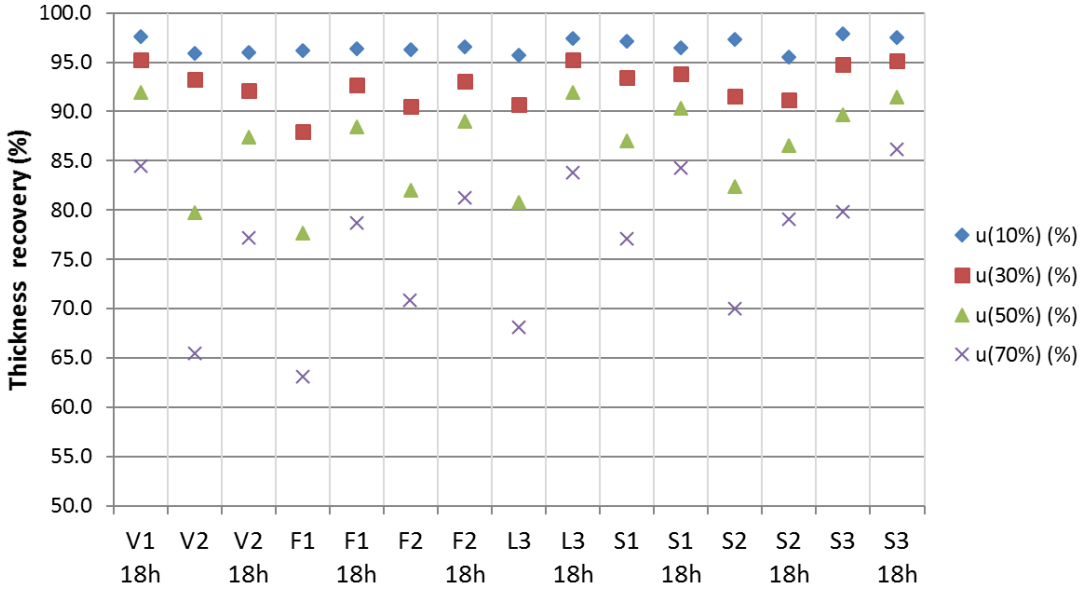

Fig. 6. Elastic recovery of the viscose samples during the cyclic compression test. Thickness determined at a pressure of 106 Pa

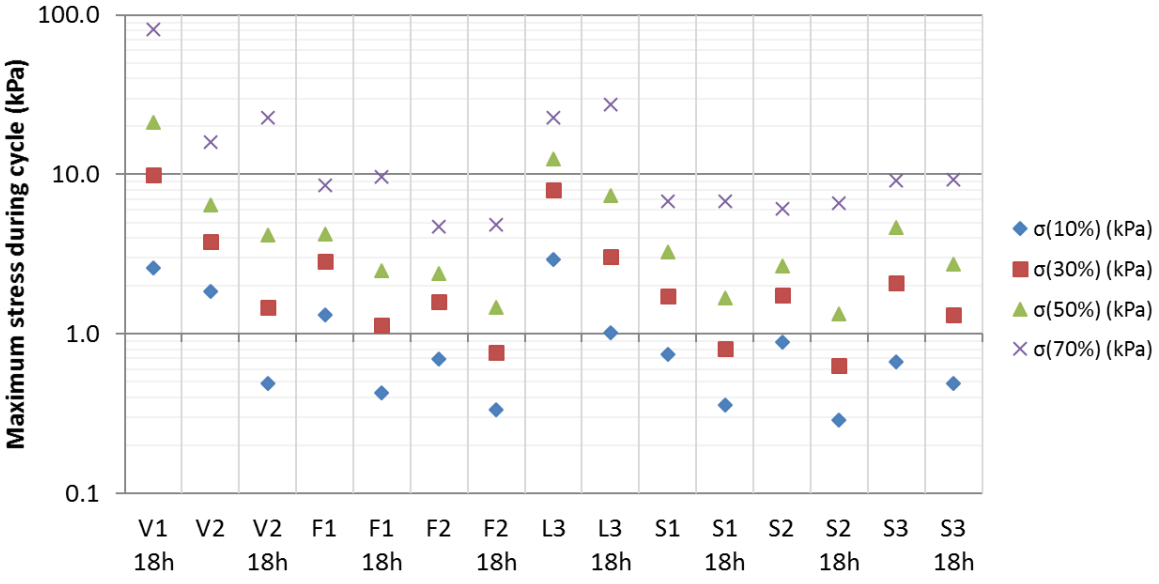

Fig. 7. Peak stress during each cycle

After 10% compression, only slight differences in the thickness recovery were observed between the samples. Each sample had a varying amount and type of defects and unevenness on the outer surface, especially on the top of the samples because of the preparation process. As the samples were tested without cutting, these defects particularly affected the 10% compression cycle. The threshold force was chosen to be as small as possible, and for some samples 10% straining may have not been enough to compress the body of the sample. For the 30%, 50%, and 70% compression cycles, the various raw material types and furnish compositions led to larger differences.

Samples V1 and V2 had a higher amount of viscose fibers and a higher density than the other samples. The first test recovery for V2 was relatively poor. For V1, the first-time recovery data is unfortunately missing. The V2 sample seemed to recover better than F1, which had half the amount of viscose, but the same composition otherwise.

Samples F1, L3, L2, and L1 had the same composition, except for a diminishing amount of (pre-vulcanized) latex. By reducing the latex amount from 14 mL (F1) to 10 mL (L3), the elastic thickness recoveries were enhanced by approximately 3% (first time tests: 30% cycle: 2.8%; 50%: 3.1%; 70%: 4.9%). The L3 sample had a poor foam quality, though. Additionally, when the latex amount was further reduced to 7 mL (L2) or removed completely from the system (L1), the samples collapsed during preparation, which demonstrated that latex was an integral component in the network. The v-fines alone were not enough to sustain the low-density network of non-binding viscose fibers. The V2 sample had double the amount of viscose fibers compared with the compositions of the four above-mentioned samples, which increased the elastic strain recovery (compared with F1). However, the decreasing amount of latex had a comparable effect on the recovery (V2 → F2).

Samples F2, S1, S2, and S3 had the same composition, but in S1, S2, and S3 the latex was vulcanized by a temperature treatment. The vulcanization temperature that was used (155 °C) is typical for crosslinking natural rubber latex with sulfur (Kato *et al.* 2015). Sulfur vulcanization causes changes at the molecular level of natural rubber, and thus changes its mechanical properties and reduces tackiness (Kato *et al.* 2015). The crosslinking density was not determined, but a clear increase in the elastic modulus of the rubber was observed with the addition of sulfur and the heat treatment. The tensile modulus of 0.98 MPa for the pre-vulcanized rubber was roughly doubled to 1.6 MPa after vulcanization with the powder sulfur and heat treatment. This treatment increased the elastic recovery for all three samples. The increase was the smallest for S2 (first time test: 30%: 1.1%; 50%: 0.5%; 70%: -1.2%) and the largest for S3 (first time test: 30%: 4.6%; 50%: 9.4%; 70%: 12.9%). Vulcanization also increased the maximum stresses, as was most clearly observed after the largest compression (70%).

The difference between S1, S2, and S3 was in the sulfur type and surfactant system. In the presence of SDS, the recoveries were better with colloidal sulfur (S1) than with powder sulfur (S2), potentially because of its easier and more even distribution into the fiber network, which consequently improved the vulcanization effect. However, both sulfur types formed macro-particles with the v-fines that were visible in the tomography images (see Fig. 4c for S2) and with the naked eye.

By adding the non-ionic surfactant to the anionic SDS, the chemistry of the wet foam became favorable for the latex to distribute evenly because of hydrophobic interactions, as was explained earlier. No visible grains were seen in the S3 dry sample. Also, the tomography images in Figs. 4a and 4b show evenly distributed latex in the fiber network. The composition still contained the same amount of v-fines, but the agglomerated

v-fines/latex particles were much smaller than in S2, as is shown in Fig. 4. Sample S3 showed a better elastic recovery than S1 and especially S2, which exceeded the elastic recoveries of all of the other samples. In the first compression test, 90% of the original thickness of S3 was recovered after the 50% cycle, and 80% was recovered after the 70% cycle. The duration of the recovery part of the cycles was 24 s and 30 s, respectively.

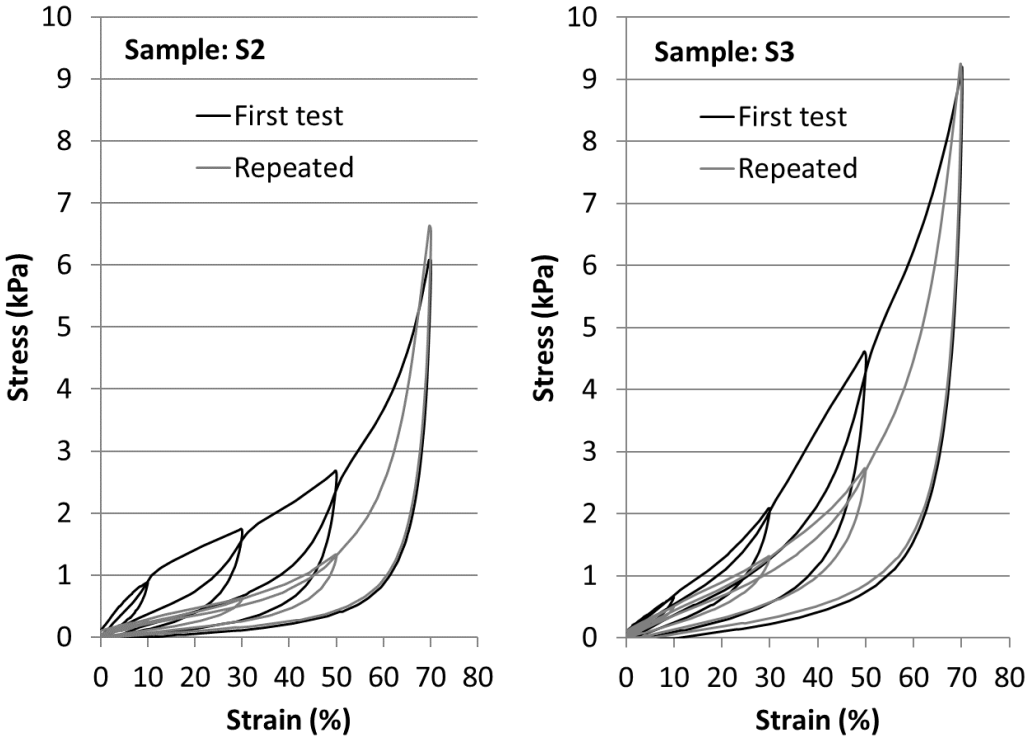

Fig. 8. Stress-strain curves of the first and repeated (after 18 h) tests for samples S2 (left) and S3 (right)

Figures 6 andFig. 7 show a prevalent and systematic difference between the first test and repeated compression test, which had a time period that was three orders of magnitude longer than the release part of the 70% cycle. In the retest, the thickness recoveries improved in the 50% and 70% cycles for all of the samples, as well as in the 30% cycle for all of the samples, except V2. The peak stress in all of the cycles below 70% for each sample was lower in the repeated test.

The effect of repeated loading can easily be observed by examining the full stress-strain curves, which are given in Fig. 8 for samples S2 and S3. The peak stresses became reduced as the whole shape of the stress-strain curve changed. During the repeated tests, a smaller compression force was required to reach a certain displacement. During the first compression tests, any brittleness that the fiber network may have had because of drying or the vulcanization heat treatment was released. In subsequent compressions, the network was able to move freely and return more easily to its original shape. This effect was very evident, such as in sample S2 (Fig. 8) where a bump in the curve occurred in the strain range from 0% to 20% and subsequently flattened out completely. Compressing the sample down to only 30% of the original thickness represented a relatively severe straining. In this case, the peak stress did not change between the first and second loading because of a relatively high compactification of the fiber network.

The deviations between the first and repeated tests suggested changes in the fiber network during compression cycles. However, no remarkable changes in the network topology, such as breaking or opening of inter-fiber bonds, were seen in the high-speed images (Fig. 9). Instead, the deformation took the form of fiber bending, which caused visible 'smooth' changes in the open porous structure.

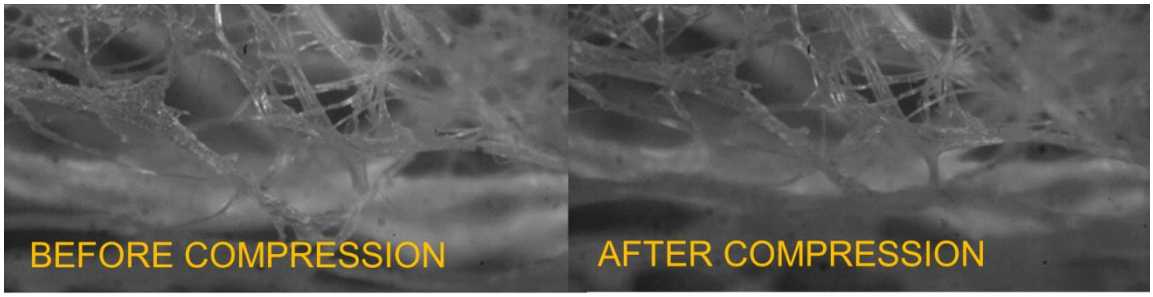

Fig. 9. High-speed images of the local fiber network of sample F2 before (left) and after (right) the first 50% compression test

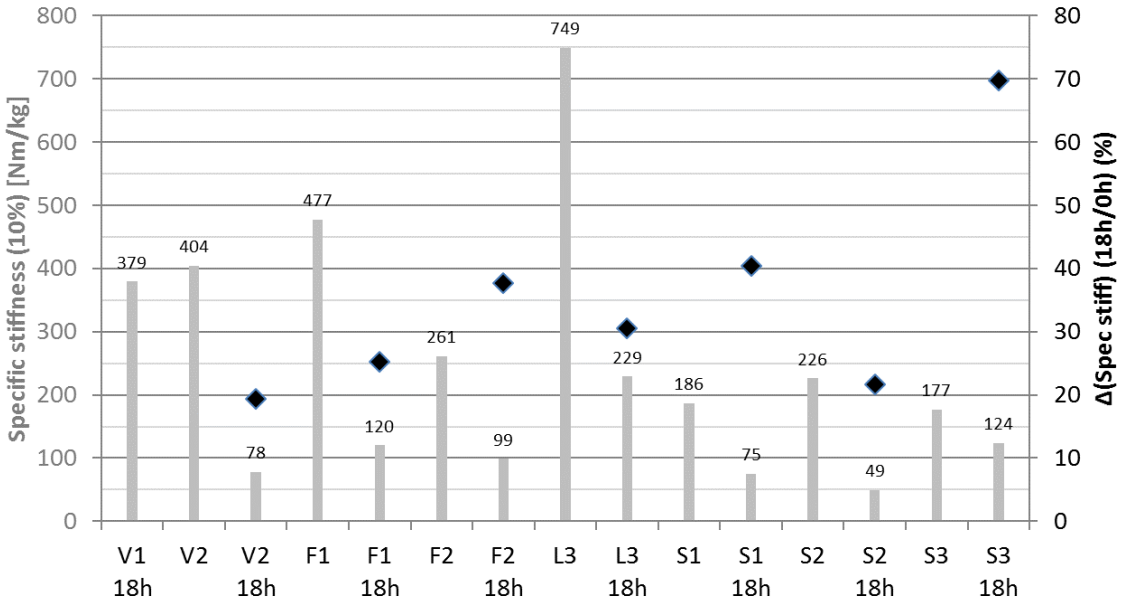

Fig. 10. Specific stiffness values from the 30% compression cycle for the viscose samples (bars), and the difference compared with the retest after 18 h (diamonds)

Figure 10 shows the specific stiffness values calculated from the 30% compression cycle. A high amount of v-fines (V1, V2, F1, and L3) increased the stiffness of the network. All of the samples lost more than half of their stiffness during the repeated test. Only sample S3 retained its stiffness well because of the even latex distribution in the fiber network.

The immediate elastic recovery data presented in Fig. 6 was produced using the 106-Pa threshold, whereas in Fig. 11, the thickness was recorded after reducing the pressure to 0 Pa and allowing a few seconds for additional creep recovery (Brezinski 1956). The obtained strain recoveries were higher for the load levels of 30%, 50%, and 70%. With the short-term creep recovery, the recorded values for the original sample thickness were 2% to 7% higher. For the 70% cycle, the values were 10% to 23% higher for the first test

and 5% to 20% higher for the repeated test compared with accounting for immediate elastic recovery only. Figure 11 also presents a long-term thickness recovery after 70% compression, which was calculated from the repeated test (after 18 h) results. During that time, the viscoelastic creep recovery was almost complete, and so all of the samples reached considerably higher total recoveries. Sample S3 reached a recovery level of 97.2%.

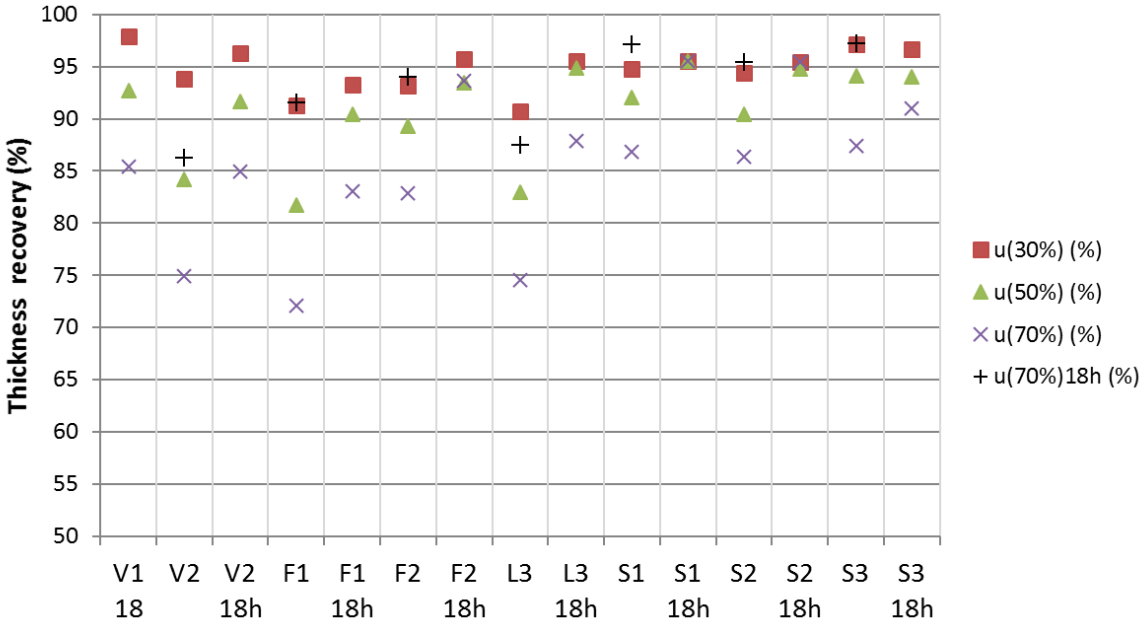

Fig. 11. Short-term creep recovery of the viscose samples for the 30%, 50%, and 70% compression tests (measured at the vanishing pressure), and long-term thickness recovery (after 18 h)

In addition to the above special model furnish, the compression recovery was also determined for a common CTMP with relatively stiff fibers and a high fines content (approx. 30%) (Fig. 12). The sample density ranged from 13 kg/m^3 to 30 kg/m^3. The latex content was around 25% for samples C5, C6, and C7, which were made with the TWEEN surfactant, whereas the reference sample C4 contained no latex. The compression levels were slightly different from the earlier series at 20%, 50%, 70%, and 90%.

Instead of measuring the immediate spring-back, the recovery was monitored over an extended period (30 s and 1800 s) after compression. At the 70% compression level at a low RH (approx. 30%), the best recovery (92%) was obtained for C6. The recovery of the initial thickness without latex was only 74% for C4.

The severe drop in the recovery for sample C5 at between 70% and 90% compression (from 89% to 55%) was probably caused by self-adhesion of the pre-vulcanized latex, which was partially released after 1800 s. The drop in the recovery was much lower for the vulcanized samples C6 and C7, as the recovery within 30 s also stayed above 70% for the 90% compression level.

For the SDS surfactant, the recovery was better for sample C3 with a small amount of latex than for C1 and C2, which had no latex. Interestingly, the surfactant type affected the recovery even without latex at an equal density. The recovery after 30 s was better for C2, which was made with SDS, than for the C4 TWEEN sample at the 50%, 70%, and 90% compression levels. However, the long-term (1800 s) creep recovery for C4 was quite high.

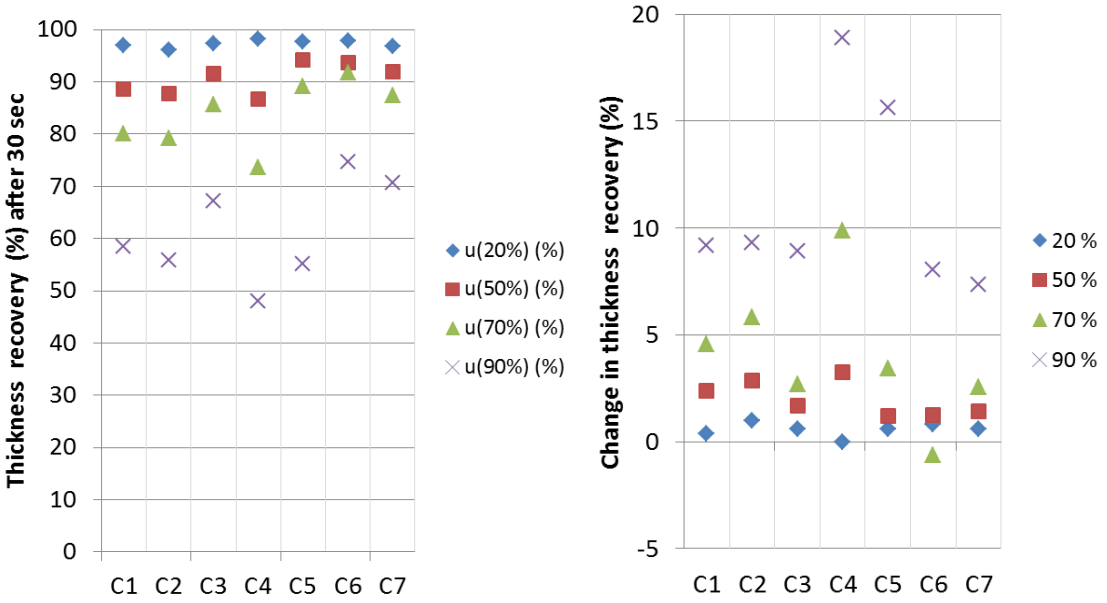

Fig. 12. Thickness recovery of the CTMP samples in the cyclic compression tests. Left: Measured after 30 s; and Right: Change in the thickness recovery from the hold times of 30 s to 1800 s

As was shown in this work, foam forming opens up the possibility of designing new properties for cellulose fiber materials. This means not only a reduction in the density or expanding the raw material space, but also enhancing key material properties, such as homogeneity, insulation, permeability, and mechanical properties. The foam forming process is compatible with very different types of materials, from long fibers to polymers. This was taken advantage of in this study by introducing an elastomeric component to the fiber network. The resulting multi-scale structure improved the compression recovery of the lightweight material. The highly porous structure of our samples required a high aspect ratio and sufficient bending stiffness of the fibres. The fines were needed to guarantee the high retention and even distribution of the latex in the structure. The study was based on somewhat artificial fiber network models, but the promising results urge further development with different types of fibers, elastomers, and foam systems.

CONCLUSIONS

1. Recovery of lightweight cellulose fiber networks after compression can be remarkably improved by the addition of elastic polymers that accumulate at the fiber joints in foam forming and drying operations.
2. Although the majority of recovery after deformation is elastic, a large proportion of the return towards the original dimensions followed the time-dependent creep recovery of the material.
3. The mechanical properties, such as the material stiffness, creep recovery, and stress-strain hysteresis, were sensitive not only to the raw material composition, but also to the foam properties (*e.g.* surfactant type).

4. High stiffness of the elastomer and an even distribution of it over the material improve compression recovery.
5. The first compression cycle relaxed the network, which led to an improved thickness recovery, but also a reduced stiffness. With subsequent compressions, the material properties changed only a little.

ACKNOWLEDGMENTS

This article was based on the results achieved in the Novel Structural Materials with Multi-scale Fibre Components (NoMa) project from 2015 to 2017. The authors are grateful for the financial support of the Finnish Funding Agency for Innovation (Tekes), VTT, the participating companies, and Lahti University of Applied Sciences. The authors would also like to thank Jarmo Kouko for the tensile measurements of the rubber samples.

REFERENCES CITED

Alava, M., and Niskanen, K. (2006). "The physics of paper," *Rep. Prog. Phys.* 69(3), 669-723. DOI: 10.1088/0034-4885/69/3/R03

Alimadadi, M., and Uesaka, T. (2016). "3D-oriented fiber networks made by foam forming," *Cellulose* 23(1), 661-671. DOI: 10.1007/s10570-015-0811-z

Al-Qararah, A. M., Ekman, A., Hjelt, T., Ketoja, J. A., Kiiskinen, H., Koponen, A., and Timonen, J. (2015a). "A unique microstructure of the fiber networks deposited from foam-fiber suspensions," *Colloid. Surf. A* 482, 544-553. DOI: 10.1016/j.colsurfa.2015.07.010

Al-Qararah, A. M., Hjelt, T., Koponen, A., Harlin, A., and Ketoja, J. A. (2015b). "Response of wet foam to fibre mixing," *Colloid. Surf. A* 467, 97-106. DOI: 10.1016/j.colsurfa.2014.11.034

Borodulina, S., Kulachenko, A., Galland, S., and Nygårds, M. (2012). "Stress-strain curve of paper revisited," *Nord. Pulp Pap. Res. J.* 27(2), 318-328. DOI: 10.3183/NPPRJ-2012-27-02-p318-328

Borodulina, S., Motamedian, H. R., and Kulachenko, A. (2016). "Effect of fiber and bond strength variations on the tensile stiffness and strength of fiber networks," *Int. J. Solids Struct*. DOI: 10.1016/j.ijsolstr.2016.12.013

Brezinski, J. P. (1956). "The creep properties of paper," *Tappi J.* 39(2), 116-128.

Flink, P., Westerlind, B., Rigdahl, M., and Stenberg, B. (1988). "Bonding of untreated cellulose fibers to natural rubber," *J. Appl. Polym. Sci.* 35(8), 2155-2164. DOI: 10.1002/app.1988.070350815

Haffner, B., Dunne, F. F., Burke, S. R., and Hutzler, S. (2017). "Ageing of fibre-laden aqueous foams," *Cellulose* 24(1), 231-239. DOI: 10.1007/s10570-016-1100-1

Heydarifard, S., Nazhad, M. M., Xiao, H., Shipin, O., and Olson, J. (2016). "Water-resistant cellulosic filter for aerosol entrapment and water purification, Part I: Production of water-resistant cellulosic filter," *Environ. Technol.* 37(13), 1716-1722. DOI: 10.1080/09593330.2015.1130174

Kak, A. C., and Slaney, M. (2001). *Principles of Computerized Tomographic Imaging*, Society of Industrial and Applied Mathematics, Philadelphia, PA.

Kato, H., Nakatsubo, F., Abe, K., and Yano, H. (2015). "Crosslinking *via* sulfur vulcanization of natural rubber and cellulose nanofibers incorporating unsaturated fatty acids," *RSC Adv.* 5(38), 29814-29819. DOI: 10.1039/C4RA14867C

Kohjiya, S., and Ikeda, Y. (2014). *Chemistry, Manufacture and Applications of Natural Rubber*, Elsevier, Cambridge, UK.

Kulachenko, A., and Uesaka, T. (2012). "Direct simulations of fiber network deformation and failure," *Mech. Mater.* 51, 1-14. DOI: 10.1016/j.mechmat.2012.03.010

Lehmonen, J., Jetsu, P., Kinnunen, K., and Hjelt, T. (2013). "Potential of foam-laid forming technology in paper applications," *Nord. Pulp Pap. Res. J.* 28(3), 392-398. DOI: 10.3183/NPPRJ-2013-28-03-p392-398

Madani, A., Zeinoddini, S., Varahmi, S., Turnbull, H., Phillion, A. B., Olson, J. A., and Martinez, D. M. (2014). "Ultra-lightweight paper foams: Processing and properties," *Cellulose* 21(3), 2023-2031. DOI: 10.1007/s10570-014-0197-3

McPherson, A. T. (1927). "Part I - Density of rubber-sulphur compounds," *Scientific Papers of the Bureau of Standards* 22, 385-397.

Nishino, T., Takano, K., and Nakamae, K. (1995). "Elastic modulus of the crystalline regions of cellulose polymorphs," *J. Polym. Sci. Pol. Phys.* 33(11), 1647-1651. DOI: 10.1002/polb.1995.090331110

Poranen, J., Kiiskinen, H., Salmela, J., Asikainen, J., Keränen, J., and Paakkonen, E. (2013). "Breakthrough in papermaking resource efficiency with foam forming," in: *Proceedings of TAPPI PaperCon*, Atlanta, GA, pp. 807-814.

Pöhler, T., Jetsu, P., and Isomoisio, H. (2016). "Benchmarking new wood fibre-based sound absorbing material made with a foam-forming technique," *Building Acoustics* 23(3-4), 131-143. DOI: 10.1177/1351010X16661564

Radvan, B., and Gatward, A. P. J. (1972). "The formation of wet-laid webs by a foaming process," *Tappi J.* 55(5), 748-751.

Saharinen, E., Nurminen, I., Salminen, L., and Leino, J. (2016). "Method and apparatus for the preparation of finely divided lignocellulosic material," Patent No. FI20145787.

Salvo, L., Cloetens, P., Maire, E., Zabler, S., Blandin, J. J., Buffière, J. Y., Ludwig, W., Boller, E., Bellet, D., and Josserond, C. (2003). "X-ray micro-tomography an attractive characterisation technique in materials science," *Nucl. Instrum. Meth. B* 200, 273-286. DOI: 10.1016/S0168-583X(02)01689-0

Stock, S. R. (2008). *MicroComputed Tomography: Methodology and Applications*, CRC Press, Boca Raton, FL.

Timofeev, O., Jetsu, P., Kiiskinen, H., and Keränen, J. T. (2016). "Drying of foam-formed mats from virgin pine fibers," *Dry. Technol.* 34(10), 1210-1218. DOI: 10.1080/07373937.2015.1103254

Zhou, Y., Fan, M., Chen, L., and Zhuang, J. (2015). "Lignocellulosic fibre mediated rubber composites: An overview," *Compos. Part B-Eng.* 76, 180-191. DOI: 10.1016/j.compositesb.2015.02.028

Article submitted: December 21, 2017; Peer review completed: February 26, 2018;
Revised version received and accepted: March 28, 2018; Published: April 18, 2018.
DOI: 10.15376/biores.13.2.4058-4074